Phytoplankton response to a plume front in the northern South China Sea

Qian P. Li [1,2,*], Weiwen Zhou [1,2], Yinchao Chen [1,2], and Zhengchao Wu[1]

[1]South China Sea Institute of Oceanology, Chinese Academy of Sciences, Guangzhou 510301, China

[2]University of Chinese Academy of Sciences, Beijing 100049, China

Corresponding to: Qian Li (qianli@scsio.ac.cn)

Abstract. Due to a strong river discharge during April-June 2016, a persistent salinity front, with freshwater flushing seaward on the surface but seawater moving landward at the bottom, was formed in the coastal waters west of the Pearl River Estuary (PRE) over the Northern South China Sea (NSCS) shelf. Hydrographic measurements revealed that the salinity front was influenced by both river plume and coastal upwelling. Shipboard nutrient-enrichment experiments with size-fractionation chlorophyll-*a* measurements were performed on both sides of the front as well as the front zone to diagnose the spatial variations of phytoplankton physiology across the frontal system. We also assessed the size-fractionated responses of phytoplankton to the treatment of plume water at the frontal zone and the seaside of the front. Biological impact of vertical mixing or upwelling was further examined by the response of surface phytoplankton to the addition of local bottom water. Our results suggested that there was a large variation of phytoplankton physiology on the seaside of the front driven by dynamic nutrient fluxes, although P-limitation was prevailing on the shore-side of the front and at the frontal zone. The spreading of plume water at the frontal zone would directly improve the growth of micro-phytoplankton, while nano- and pico-phytoplankton growths could become saturated at high percentages of plume water. Also, the mixing of bottom water would stimulate the growth of surface phytoplankton on both sides of the front by altering the surface N/P ratio closer to the Redfield stoichiometry. In summary, phytoplankton growth and physiology could be profoundly influenced by physical dynamics of the frontal system during the spring-summer of 2016.

1 Introduction

It is well known that physical dynamics of the coastal ocean can be strongly influenced by river input. When there is a high river discharge, a large plume of brackish water can form near the estuary mouth and the adjacent inner shelf regions, which is generally a low-salinity mesoscale feature that disperses fresh river water across the coastal margin (Horner-Devine et al., 2015). River plumes can transport and redistribute river-borne materials, such as nutrients and particles, and thus largely affect biogeochemistry of the coastal ocean (Dagg et al., 2004; Lohrenz et al., 2008). Convergent surface fronts over the shelf are a common feature associated with river plumes (e.g. Garvine and Monk, 1974). These plume-induced fronts are often the places of high phytoplankton productivities (Acha et al., 2004) and thus provide important feeding and reproductive habitats for higher trophic-level marine organisms, such as zooplankton and fish (Morgan et al., 2005).

Biological production of the coastal Northern South China Sea (NSCS) is controlled by monsoon-driven upwelling that brings nutrient-rich deep waters to the shelf (Liu et al., 2002). In addition, there is an intense river discharge from the Pearl River Estuary (PRE) during the spring-summer leading to the development of a strong river plume nearshore (Su, 2004). In the coastal water west of the PRE, convergence between the northeastward coastal current and the southeastward river plume can maintain a sharp salinity front along the shelf when the southwest monsoon is prevailing over the region (Wong et al., 2003). Variability of the front is primarily controlled by the river discharge and by the direction and magnitude of the regional wind field (Dong et al., 2004). On the east of the PRE, the surface plume water can be entrained in the coastal current as a salinity tongue in the summer and propelled eastward and offshore by wind-driven jets to affect a large area of the NSCS shelf-sea (Gan et al., 2009).

The plume front over the NSCS shelf creates an interface between the river plume and the adjacent marine waters with rapid changes of both salinity and nutrients at the frontal zone (e.g. Cai et al., 2004). There is a P-limitation of phytoplankton growth in the river plume due to a high N/P ratio of the PRE water (Zhang et al., 1999; Yin et al., 2001). In contrast, biological production is generally N-limited in the offshore oceanic waters (Wu et al., 2003; Chen et al., 2004), as the upwelled deep-water with an N/P

ratio of ~14 is essentially N-deficient compared to the Redfield N/P ratio of 16 (Wong et al., 2007). A shift from P-limitation to N-limitation of phytoplankton community across the plume edge to the sea has been speculated based on results of the Hong Kong waters (Yin et al., 2001). Results of a physical-biogeochemical coupling model in the NSCS indeed predict a fast decrease of N/P ratio from ~120 in the near-field to <13.3 in the far-field of the plume front driven by a higher N/P consumption ratio and by mixing with the ambient lower N/P water (Gan et al., 2014).

Nutrient variations, in addition to light fluctuation, can affect the partitioning of phytoplankton biomass between different size classes (Marañón et al., 2012, 2015). The change of phytoplankton size structure can be controlled by size-dependent trade-off processes for resource acquisition and use (Marañón, 2015). Small phytoplankton has a higher nutrient affinity for growth under nutrient limiting conditions (Suttle, 1991; Raven et al., 1998), whereas large phytoplankton shows higher growth efficiency under favorable nutrient conditions (Cermeño et al., 2005). A large shift of phytoplankton assemblage from small to large cells could arise following the addition of nutrients from deep seawater in the North Pacific Subtropical Gyre (McAndrew et al., 2007; Mahaffey et al., 2012). The success of large phytoplankton in the oligotrophic ocean would highly depend on external environmental dynamics, although it has the metabolic potential of enhancing production (Alexander et al., 2015). It is thus important to understand not only the mechanisms for nutrient variations but also the response of size-fractionated phytoplankton community to the diverse nutrient supplies, particularly at the frontal zone where the patchiness of phytoplankton can be affected by complex physical dynamics (Li et al., 2012).

Three field surveys were carried out to study the biological response to a strong salinity front over the NSCS shelf during the April-June of 2016. Besides comprehensive hydrographic and biogeochemical measurements, such as temperature, salinity, nutrients, and chlorophyll-*a*, we performed nutrient-enrichment experiments with size-fractionation chlorophyll-*a* measurements at the shore-side, the frontal zone, and the seaside of the front to examine the spatial change of phytoplankton physiology. Phytoplankton response to the river plume at the frontal zone was addressed by mixing the local surface water with a varying percentage of plume water from the shore-side of the front. The

impact of river plume on the seaside of the front was further examined by incubations of the surface seawater with the treatment of plume water. In addition to these experiments, the bottom water was added to the surface water for incubation at various zones of the frontal system to estimate the impact of vertical mixing or upwelling on surface phytoplankton community. We hope to use these experimental approaches to address the responses of phytoplankton growth and physiology to the strong salinity front over the shelf. Based on these field results, we will also discuss the impacts of river plume, vertical mixing and coastal upwelling on physical and biogeochemical dynamics of the frontal systems in the NSCS shelf-sea.

2. Material and methods

2.1 Description of the field work

Three field cruises aboard *R/V Zhanjiang Kediao* were performed during April, May, and June in 2016 with hydrographic and biogeochemical samplings over the NSCS shelf (Fig.1). A vertical transect across the salinity front from the inner estuary to the shelf was intensively sampled during the June (Section A in Fig. 1). There were three other transects (Section B, C, and D in Fig. 1) outside the PRE with intense size-fractionation chlorophyll-*a* measurements during both May and June. Section B transited across the frontal zone with Sections C and D on the seaside of the front. Surface waters at different zones of the salinity front were selected for nutrient-enrichment experiments, including the shore-side of the front (S1 and S2), the frontal zone (S3 and S4), and the seaside of the front (S5, S6, and S7) during May and June 2016. Station S8 is located at the same place as S4 but 9 days later.

2.2 Measurements of hydrography, chlorophyll-a, nutrients and phytoplankton size structure

Seawater temperature, salinity, pressure, and fluorescence were acquired using a SeaBird model SBE9/11 conductivity-temperature-depth (CTD) recorder and a Chelsea Aqua fluorometer. Discrete water samples at 1m, 20m, 40m, 60m, 80m, and 100m were collected with Niskin bottles mounted onto a Rosette sampling assembly (General Oceanic). After filtration onto a Whatman GF/F glass fiber filter,

the chlorophyll-*a* (Chl-*a*) sample was extracted by 90% acetone in darkness at 4°C for 24 h and determined using a Turner Design fluorometer (Knap et al., 1996). Three types of filters (20 µm Nylon filter, 2 µm Polycarbonate filter, and 0.7 µm GF/F filter) were used to produce three different size-classes including micro- (>20 µm), nano- (2-20 µm), and pico-phytoplankton (0.7-2 µm). Nutrient samples were collected inline through a Whatman GF/F filter and frozen immediately at -20°C until analyzed. After thawing at room temperature, they were analyzed by an AA3 nutrient auto-analyzer using colorimetric methods (Knap et al., 1996) with detection limits of 0.02, 0.02, and 0.03 $\mu mol\ L^{-1}$, for nitrate plus nitrite (N+N), soluble reactive phosphate (SRP), and silicate (Si), respectively.

2.3 Setup of the shipboard incubation experiments

There were four different treatments prepared in duplicate for nutrient-enrichment experiments including the control (C), nitrogen alone (+N), phosphorus alone (+P), and nitrogen plus phosphorus (+NP). Nutrients were added to the incubation bottle based on the Redfield N:P ratio to obtain final concentrations of 4.8 µM $NaNO_3$ and 0.3 µM NaH_2PO_4. Seawater samples were prescreened through a 200 µm mesh to remove large grazers. These samples were incubated in 2.4 L transparent acid-cleaned polycarbonate bottles and placed in a shipboard incubation chamber equipped with a flow-through seawater system. The incubator was shaded to mimic 30% sunlight using a neutral filter with each bottle manually stirred twice a day. Nutrient addition experiments were performed at S1, S3, S5 during May 2016 and S2, S4, S6, S7, S8 during June 2016 (Table 1). Each incubation experiment was conducted immediately upon reaching the station and lasted for two days with size-fractionated chlorophyll-*a* and nutrient samples taken once a day.

Surface water (~50L) collected at S2 outside the PRE mouth was saved as the plume water (PW). Half of the PW was filtered through a 0.2 µm Millipore membrane filter (GTTP Isopore^{TM}) to produce the filtered plume water (FPW). The FPW was used to dilute the local surface waters at S6, S7, and S8 by a fraction of 12.5%. At station S6, the raw plume water (PW) was also added to the surface water for incubation to test the possible advective chlorophyll input by the river plume. Under the in-situ temperature and light, the mixture was incubated on board for two days with size-fractionation

chlorophyll-*a* collected each day. In order to examine the response of a mixed phytoplankton community at the frontal zone to various mixing conditions driven by the dispersive river plume, we also conducted a series of mixing experiments between surface waters of S2 and S4 on June 19th, 2016, with the final percentages of S4, 25% S2 + 75% S4, 50% S2 + 50% S4, 75% S2 + 25% S4, and S2 corresponding to the final salinity of 30.7, 24.7, 18.7, 12.7, and 6.6, respectively. The bottom waters (BW) were collected at S2, S4, S6, and S7 and stored in clean HDPE carboy. A 0.2-μm-filtration was used to create the filtered bottom water (FBW). Both BW and FBW, with a final percentage of 12.5%, were added to the local surface water for incubation to study the impact of vertical mixing or upwelling on phytoplankton growth at these stations.

For each size class, the rate of daily chlorophyll-*a* production ($\mu g\ L^{-1}\ d^{-1}$) was calculated by the difference of size-fractionated chlorophyll-*a* concentration during each incubation day. We also estimated the net growth rates μ (d^{-1}) for the water mixing experiment between S2 and S4 by μ $=ln(Chl_1/Chl_0)/\Delta t$, with Chl_0 and Chl_1 the initial and final size-fractionated chlorophyll-*a* concentrations every day ($\Delta t =1$ day). The specific growth rate approach could not work for other experiments, as large errors of μ would arise when the initial chlorophyll-*a* of a certain size-class (Chl_0) was close to zero.

2.4 Estimations of horizontal advection and vertical mixing at the seaside of the front

Assuming a salinity balance at the seaward front (Fong and Geyer, 2001), we have

$$U_e(S_0 - S) = K_H \frac{\partial S}{\partial z} \tag{1}$$

where S and S_0 are salinity of the plume front and ambient water, K_H is the eddy diffusivity, and the bulk entrainment rate U_e is computed by $U_e \approx 0.038 Ri^{-0.5}(\tau/\rho)^{0.5}$ with the Richardson number (Ri) given by

$$Ri = \frac{g\rho}{\tau\rho_0} \int_0^h (\rho_0 - \rho)dz \tag{2}$$

with g the gravitational acceleration, ρ_0 the ambient density, h the thickness of plume front and τ the wind stress (Fong and Geyer, 2001).

Horizontal nitrate flux to the surface water on the seaside of the front can thus be estimated by $J_h = U_e (N - N_0)$ with N and N_0 the nutrient concentrations of the plume front and the ambient water. The vertical nitrate flux can be estimated by $J_v = K_H (\partial N/\partial z)$.

3 Results

3.1 Physical and biogeochemical setting of the NSCS shelf during the spring-summer

The temperature versus salinity diagram revealed a large change of hydrography during the three cruises (Fig. 2). There was a regional increase of temperature over shelf from April to June (Fig. 3A1-A3), along with the increase of wind strength (with a regional shift to upwelling favorable wind after the May, data not shown). The riverine input was clearly evidenced with low salinity waters in all the three cruises (Fig. 2). Spatially, there was a large area of low salinity in the coastal water west of the PRE (Fig. 3B1-B3), leading to a strong salinity front in the inner shelf. The plume water was mostly on the shore side of the front when the river-outflow flowing westward along the shore. The shore-side of the front was defined by a salinity of <26, the nearshore boundary of the plume (Wong et al., 2003), with the seaside of the front by a salinity of >32, the offshore boundary of the plume (Ou et al., 2007). The frontal zone is thus located in between the nearshore and offshore boundaries of river plume (Fig. 1).

In the coastal water west of the PRE, there was an intense chlorophyll-a bloom (Chl-a > 5 μg/L) on the shore-side of the front during all the three cruises (Fig. 3C1-C3), although the surface temperature of the bloom area increased from ~22°C in April, to ~26°C in May and to ~31°C in June. The surface distributions of nitrate, silicate, and phosphate generally follow that of salinity for all the three cruises with much higher concentrations on the shore-side of the front than the seaside of the front (Fig. 3D and 3F). Interestingly, the surface low salinity tongue in the coastal water east of the PRE (generated by eastward plume dispersion) was cut off by another water mass of low temperature but

high salinity during the June (Fig. 3A3 and 3B3). This colder and saltier water presumably should come from the subsurface via coastal upwelling, which was further supported by its higher phosphate concentration but lower N/P ratio compared to the ambient waters (Fig. 3D3 and 3F3).

There were substantial vertical changes in temperature, salinity, and chlorophyll-*a* while crossing the salinity front (Fig. 4A-4C) from the estuary to the shelf (Section A). The surface front was located in the inner shelf with the subsurface frontal zone going deep to the bottom of the estuary mouth (Fig.4A). Vertical distributions of nutrients generally followed that of salinity in the PRE with higher surface concentrations, whereas there was large drawdown of nutrients on the shore-side of the front when approaching the edge of the river plume (Fig. 4D-4F), corresponding to a fast decrease of N/P ratio from the shore-side of the front to the frontal zone. The dominant size-class shifted from micro- to pico-cells while crossing the salinity front from the shore in Section B for both the May and June cruises (Fig. 5). Variations in the percentages of micro- and nano-cells in Sections C and D were due to a spatial change of the frontal zone (Fig. 5).

3.2 Variations of phytoplankton nutrient limitation over the NSCS shelf

Surface water properties of the incubation stations were summarized in Table 1. The highest concentrations of nutrients and chlorophyll-*a* were in S1 and S2 on the shore-side of the front where micro- and nano-cells dominated. A P-deficiency of the plume water can be inferred from the high N/P ratios there. There was higher salinity (~30) but lower chlorophyll-*a* (~1 µg/L) in S3 and S4 at the frontal zone, which should reflect a reduced impact of river plume. The surface waters of S5, S6, and S7 on the seaside of the front were dominated by pico-phytoplankton and showed the typical characteristics of the open NSCS with low nutrients and chlorophyll-*a* but high salinity.

Phytoplankton total chlorophyll-*a* on the shore-side of the front (S1 and S2) and at the frontal zone (S3 and S4) showed responses to P-addition but not N-addition, suggesting P-limitation in these waters (Fig. 6A1-6D1). Results of nutrient variations during the incubations confirmed that N consumptions in these stations were significantly enhanced by the addition of P (Fig. 6A2-6D2), but P consumptions

were not stimulated by the addition of N (Fig. 6A3-6D3). In contrast, phytoplankton nutrient limitation varied substantially at S5, S6, and S7 on the seaside of the front (Fig. 6E1-6G1). Total chlorophyll showed no response to N-addition, P-addition, and N-plus-P addition at S5 (Fig. 6E1), which should suggest a relief of phytoplankton community from N- and P-stresses there. Indeed, there was no difference in nutrient consumption between N and P additions (Fig. 6E2 and 6E3) There was an N-limitation of phytoplankton at S6, as the total chlorophyll-*a* increasing with N-addition but not with P-addition (Fig. 6F1), which was consistent with its low N+N concentration of <0.5 μM at the surface (Table 1). The N-limitation of S6 was further supported by nutrient data with enhanced P consumption by N addition in Fig. 6F3 (but no difference of N consumption by P addition, Fig. 6F2). Phytoplankton growth was P-limited at S7 during the first day of incubation (Fig. 6G1 and 6G2), but it became co-limited by both N and P during the second day of incubation (Fig. 6G1) as the substrate N was running out (Fig. 6G2). This station (S7) was on the shelf edge, far away from the frontal zone, but was influenced by the eastward extension of the plume as indicated by its relatively low surface salinity.

Interestingly, the response of phytoplankton total chlorophyll-*a* to nutrient treatment was mostly mediated by micro-cells at stations S1, S2, and S3 where high nutrient concentrations and N/P ratios were found (Fig. 6A4-6C4). In contrast, for stations S5, S6 and S7 on the seaside of the front, the change of phytoplankton total chlorophyll-*a* at the surface layer was largely contributed by pico-phytoplankton (Fig. 6D4-6G4). This result is consistent with the contention that larger phytoplankton grows faster than small cell under nutrient-replete conditions.

3.3 Responses of surface phytoplankton to the addition of plume water

We considered the mixing of both nutrients and phytoplankton between the plume water and the local seawater at the frontal zone, given the relatively short distance of these two waters. The result of mixing experiments between the surface waters of S2 and S4 was shown in Fig.7. The total chlorophyll-*a* of the mixed phytoplankton community was proportional to the amount of PW (the surface water of S2) (Fig. 7A), as the PW had more chlorophyll-*a* than S4 (Table 1). Given a P-limitation of the mixed phytoplankton community, the substrate phosphate was quickly consumed within the first day of

incubation (Fig. 7B). The three phytoplankton size-classes showed distinct responses to the ascending PW percentage during the first day of incubation (Fig. 7C and 7D). There was a linear increase of the daily chlorophyll-*a* production rate of micro-cells with the percentage of PW (r^2=0.9, p<0.01), whereas the production rate of nano-cells first increased with the PW percentage from 0% to 50% and then remained relatively stable from 50% to 100%. Apart from both micro- and nano-cells, pico-phytoplankton reached the maximal production rates at 50-75% of PW treatments. The responses of net growth rates to various PW treatments (Fig. 7D) were slightly different from those of the chlorophyll-*a* production rates (Fig. 7C). The net growth rate of micro-phytoplankton increased with the PW percentage before becoming saturated at 75-100% PW. Pico-phytoplankton showed a higher net growth rate but lower daily chlorophyll-*a* production rate than nano-phytoplankton during the first day of incubation in the cases of 50-100% PW treatments. As the phosphate was running out (Fig. 7B), there were negative net growth rates for all the size-classes during the second day of incubation (Fig. 7D).

The chlorophyll-*a* biomass, as well as the daily chlorophyll-*a* production rate, was substantially enhanced by the addition of FPW at S6, S7, and S8 (Fig. 8A1-8C1), regardless the type of nutrient limitation the surface phytoplankton originally experienced. This should be expected as the plume water had much more nutrients than the local waters on the seaside of the front (Fig. 8A2-8C2 and Fig. 8A3-8C3). The small percentage of FPW addition (12.5%) was to ensure that the initial chlorophyll-*a* concentration after FPW dilution is comparable with that of the control experiment (thus, the initial chlorophyll-*a* will neither be promoted by the addition nor be diluted too much by the addition). The response of phytoplankton community to FPW was largely determined by nano- and pico-cells at these stations (Fig. 8A4-8C4). Interestingly, although the amount of the raw plume water (PW) added was only 12.5%, it contributed about half of the chlorophyll biomass to the mixed community for S6, which was due to the high chlorophyll-*a* concentration of PW (Table 1). That is why a stronger response of phytoplankton chlorophyll-*a* to PW than to FPW was observed (Fig. 8A1).

3.4 Responses of surface phytoplankton to the addition of bottom waters

The addition of FBW increased the total chlorophyll-*a* of S2, which was largely contributed by micro-cells (Fig. 9A1 and 9A4). At this station, the inclusion of FBW (a lower N/P ratio of ~28) reduced the N concentration (Fig. 9A2) but not P concentration (Fig. 9A3), leading to a lower N/P ratio of the surface water (~87) and thus the P-stress of surface phytoplankton. We found no difference in chlorophyll responses to FBW and BW at S2, which could be due to the low chlorophyll-*a* of BW. Interestingly, there was a net loss of phytoplankton chlorophyll-*a* with time at S4, which was not affected by the FBW treatment (Fig. 9B1). This is because nitrate and phosphate concentrations of the surface water were similar to those of the FBW, although there was a 9-fold increase of silicate in the FBW (Table 1). The elevated silicate after FBW treatment did not stimulate a diatom growth given the sparse of micro-cells in the surface water there. The addition of BW substantially decreased the total chlorophyll-*a* (Fig. 9B1), although the consumptions of N and P were similar to those of the control (Fig. 9B2 and 9B3). Both the additions of FBW and BW were found to stimulate phytoplankton growth at S6 (Fig. 9C1) due to elevated N concentration (Fig. 9B2), whereas the magnitude of promotion by FBW is much higher than that by BW (Fig. 9C1). There was no significant difference found in growth responses of phytoplankton to FBW and BW treatments at S7 (Fig. 9D1). This is because the BW of S7 was from the depth of 109 m with higher nutrients but negligible chlorophyll-*a* compared to the surface water (Fig. 9D1-9D3).

4 Discussion

The persistent salinity front we observed from April to May of 2016 was a plume-induced buoyant front (e.g. Ou et al., 2007), which could appear when the freshwater discharge was much stronger than the tidal effect (Garvine and Monk, 1974). While governed by buoyancy, planetary rotation, and wind forcing (Wong et al., 2003), the impact of the plume front on the coastal NSCS was large, as the low salinity water spreading westward and eastward onto the large area of the shelf. A chlorophyll bloom on the shore-side of the front was a direct response of phytoplankton to the river plume (Harrison et al., 2008), as nutrient replenishment from the subsurface could be restricted by the salinity front with a persistent stratification at the frontal zone. On the other hand, there was an intense upwelling found near

the coastal water east of the PRE, which could be due to an intensified cross-isobath transport of the bottom boundary layer driven by an amplified alongshore current (Gan et al., 2009). Therefore, the frontal system was affected by both river plume and coastal upwelling during the spring-summer of 2016.

Phytoplankton growth over the shore-side of the front was essentially P-limited, which is consistent with previous findings (Zhang et al., 1999; Yin et al., 2001). Phytoplankton P-stress here is a physiological response to the P-deficiency of the river plume due to the stoichiometric lack of P relative to N (Moore et al., 2013). However, we found a spatial difference of phytoplankton physiology on the seaside of the front, where there was less influence of river plume from the perspective of salinity. Phytoplankton growth over the seaside of the front, dominated by small pico-cells, could be P-limited, or N-limited, or not limited by N and P. There was no evidence of Si-limitation since micro-cell was not stimulated by the filtered bottom water with a much higher silicate concentration. The spatial difference of phytoplankton physiology is consistent with the nutrient variation of the developing plume front, which should be regulated by both biological uptake and physical dynamics (Gan et al., 2014).

A balance between horizontal advection and vertical mixing can be approximately maintained at the seaward front by an Ekman straining mechanism (Fong and Geyer, 2001) with salinity gradients created by cross-shore Ekman current but destroyed by vertical mixing. Based on the hydrographic data, we can estimate a horizontal entrainment rate U_e of 0.5-1.0×10^{-5} m/s and a vertical diffusivity K_H of 0.8-1.7×10^{-4} m^2/s across the frontal boundary, which are comparable to those previously found over the NSCS shelf (St. Laurent, 2008; Li et al., 2016). Horizontal nitrate flux to the seaside of the front is thus 0.2-3.6 mmolN/m^2/d. If we assume the same K_H for the seaside of the front, we can also roughly estimate a vertical nitrate diffusive flux of 0.6-4.7 mmolN/m^2/d, which is on the same order of magnitude as the horizontal nutrient fluxes. Therefore, the varying nutrient supply driven by physical dynamics, including cross-front advection and vertical mixing, might be responsible for the variability of phytoplankton physiology on the seaside of the front.

Phytoplankton community at the frontal zone during our mixing experiment between S2 and S4 should be consist of coastal phytoplankton species, as the salinity of 6.6-30.7 is higher than the lethal

level of ~5 for most estuarine phytoplankton due to osmotic pressure (Kies, 1997; Flöder et al., 2010). Coastal phytoplankton would generally tolerate a much larger range of salinity than estuarine and oceanic species (e.g. Brand 1984). Therefore, the salinity effect could be less important for the change of chlorophyll-*a* concentration during our experiments. The observed chlorophyll-*a* response of the mixed community to the PW treatments at the frontal zone should reflect the combined effects of varying nutrient concentrations and phytoplankton populations induced by the addition of PW. The relative contributions of these two factors were roughly assessed at station S6 with the additions of a small percentage (12.5%) of FPW and PW, respectively (Fig. 8A1-8A4). Due to a large increase of initial nutrient concentrations by the addition of FPW, phytoplankton growth was significantly enhanced compared to that of the control experiment with a similar initial chlorophyll-*a* concentration. A stronger chlorophyll-*a* response to the PW treatment than to the FPW treatment at S6, however, was caused by an enhanced initial phytoplankton population by PW, which also resulted in a larger nutrient drawdown during the PW addition experiment (Fig. 8A2-8A3).

The mixing of plume water at the frontal zone was found to directly stimulate micro-phytoplankton growth, while a community P-limitation was still prevailing. Although the growths of nano- and pico-cells were improved by low percentages of PW (<50%), they were inhibited by high percentages of PW (>50%). The finding is consistent with the different nutrient uptake kinetics of the three phytoplankton size-classes (Finkel et al., 2009). Micro-phytoplankton generally has a larger half-saturation constant for nutrient uptake than nano- and pico-phytoplankton (Cermeno et al., 2005; Litchman et al., 2007). Therefore, small phytoplankton (nano- and pico-cells) could become saturated with the ascending nutrients before micro-phytoplankton did. At the frontal zone, nano-phytoplankton growth even well exceeded micro-phytoplankton at a low percentage of PW (<50%), which could explain the enhanced biomass percentage of nano-cells at the frontal zone. The difference of chlorophyll-*a* production and net growth rate among three phytoplankton size-classes could also be related to the change of seawater N/P ratio. It has been known that the optimal N/P ratio of phytoplankton may vary substantially among different phytoplankton species (Geider and Roche 2002) and may increase with ascending N/P of the available nutrients (Hillebrand et al., 2013). Faster-growing small phytoplankton, such as cyanobacteria, often has a lower optimal N:P ratio leading to its

domination in eutrophic waters with lower N/P ratios (Vrede et al., 2009; Hillebrand et al., 2013), which is consistent with our finding of reduced net growth rates of small phytoplankton at higher percentages of PW treatments (higher N/P ratios).

Different from the shore-side of the front with a sharp decrease of nutrients at depths, the bottom water on the seaside of the front showed much higher nutrient concentrations (but lower N/P ratios) than the surface water, which was due to the intrusion of the deep water (Gan et al., 2014). Thus, surface nutrient concentrations after vertical mixing or upwelling should decrease on the shore-side of the front but increase on the seaside of the front. The final consequence of vertical mixing on both sides of the front was to alter the N/P ratio of surface water closer to the Redfield ratio of 16 and thus improved the growth of phytoplankton. Indeed, phytoplankton growth was substantially promoted by the FBW addition at S6 (Fig. 9C1), as the N-stress of phytoplankton was relieved by the FBW with higher nitrate concentration (Fig. 9C2) and N/P ratio (Fig. 9C3). At station S7, both FBW and BW additions increased surface phytoplankton growth (Fig. 9D1), which could be attributed to a reduced P-stress of phytoplankton in response to a lower N/P ratio (~29) of the surface water. While microplankton growth was slightly stimulated by BW addition, our results on the seaside of the front did not show a shift of phytoplankton community from pico- to micro-cells in response to upwelled nutrients from deep-water-additions found in the western South China Sea (Cui et al., 2016) and in the open ocean (McAndrew et al., 2007; Mahaffey et al., 2012).

In addition to nutrient stresses by varying nutrient concentrations and ratios, phytoplankton growth at the frontal zone should also be influenced by other factors such as the change of grazing pressure (Li et al., 2012). There was indeed evidence of enhanced grazing activity at stations S4 and S6 when comparing incubation results of the filtered bottom water (BW) with those without filtration (FBW). We found a reduced phytoplankton growth with the addition of BW compared to that of FBW at both S4 and S6 (Fig. 9B1 and 9C1). The finding should indicate of an intense grazing activity of BW since both N and P consumptions were very similar between BW and FBW treatments at these stations (Fig. 9B-9C). Therefore, a further study of grazing impact of zooplankton on various sizes of phytoplankton and subsequent biomass accumulation at the frontal zone of the NSCS shelf may be a future research

priority. Since we have only focused on phytoplankton physiology of the surface layer, the future study may also need to address the response of subsurface phytoplankton community to the frontal dynamics over the shelf, since both the light field and nutrient conditions may vary substantially at the subsurface layer across the salinity front.

5 Conclusions

Overall, the importance of physical-biological interaction in driving the patterns of phytoplankton physiology and size-fractionated growths within a strong plume-induced salinity front over the NSCS shelf was investigated by intense field measurements and shipboard incubation experiments during April-June 2016. The current study suggested that variability of phytoplankton nutrient limitation and size-fractionated growth on the shore-side, the seaside, and the frontal zone of the shelf-sea frontal system could be attributed to varying nutrient supplies driven by physical dynamics of the frontal system. While the impact of river plume was to directly increase the growth rates of all the three phytoplankton size-classes, both nano- and pico-cells could become saturated with a high percentage of plume water at the frontal zone. Vertical mixing or upwelling was found to substantially improve surface phytoplankton growth on both sides of the front by altering the nutrient concentrations and ratios. These results are important for a better understanding of the physical control of coastal ecosystem dynamics in the NSCS shelf-sea.

Acknowledgements

We thank the captain and the staffs of *R/V Zhanjiang Kediao* for help during the cruises. Drs Jie Xu and Dongxiao Wang were acknowledged for cruise assistants. This work is supported by the National Key Research and Development Program of China (2016YFC0301202) and the National Natural Science Foundation of China (41676108, 41706181).

Reference

Acha, E.M., Mianzan, H.W., Cuerrero, R.A., Favero, M., and Bava, J.: Marine fronts at the continental shelves of austral South America: Physical and ecological processes, J. Mar. Syst., 44, 83-105, 2004.

Alexander, H., Rouco, M., Haley, S.T., et al.: Functional group-specific traits drive phytoplankton dynamics in the oligotrophic ocean, PNAS, 112, 5972–5979, 2015.

Brand, L.E.: The salinity tolerance of fourty-six marine phytoplankton isolates, Estuar. Coast. Shelf Sci., 18, 543-556, 1984.

Cai, W., Dai, M., Wang, Y., et al.: The biogeochemistry of inorganic carbon and nutrients in the Pearl River estuary and the adjacent Northern South China Sea, Cont. Shelf Res., 24(12), 1301-1319, 2004.

Cermeño P, Maranón, E., Rodríguez, J., et al.: Large-sized phytoplankton sustain higher carbon specific photosynthesis than smaller cells in a coastal eutrophic ecosystem, Mar. Ecol. Prog. Ser., 297, 51-60, 2005.

Chen Y.L.L., Chen, H.Y., Karl, D.M., and Takahashi, M.: Nitrogen modulates phytoplankton growth in spring in the South China Sea, Cont. Shelf Res., 24, 527-541, 2004.

Cui, D., Wang, J., and Tan, L.: Response of phytoplankton community structure and size-fractionated chlorophyll-a in an upwelling simulation experiment in the western South China Sea . J. Ocean Univ. China, 15(5), 835-840, 2016.

Dagg, M.J., Benner, R., Lohrenz, S.E., and Lawrence, D.: Transformation of dissolved and particulate materials on continental shelves influenced by large rivers: plume processes, Cont. Shelf Res., 24, 833-858, 2004.

Dong, L., Su, J., Wong, L., Cao, Z., and Chen J.: Seasonal variation and dynamics of the Pearl River plume, Cont. Shelf Res., 24(16), 1761–1777, 2004.

Finkel, Z.V., Beardall, J., Flynn, K.J., Quigg, A., Rees, T.A.V., and Raven, J.A.: Phytoplankton in a changing world: cell size and elemental stoichiometry, J. Plankton Res., 32(1), 119–137, 2010.

Flöder, S., Jaschinski, S., Wells, G., and Burns, C.W.: Dominance and compensatory growth in phytoplankton communities under salinity stress, J. Exp. Mar. Bio. Eco., 395(1-2), 223-231, 2010.

Franks, P.J.S.: Phytoplankton blooms at fronts: patterns, scales, and physical forcing mechanisms, Rev.

Aqua. Sci., 6, 121-131, 1992.

Fong, D.A., and Geyer, W.R.: Response of a river plume during an upwelling favorable wind event, J. Geophys. Res., 106(C1), 1067-1084, 2001.

Gan, J., Cheung, A., Guo, X., and Li, L.: Intensified upwelling over a widened shelf in the northeastern South China Sea, J. Geophys. Res., 114, C09019, doi: 10.1029/2007JC004660, 2009.

Gan, J., Lu, Z., Cheung, A., Dai, M., Liang, L., Harrison, P.J., and Zhao X.: Assessing ecosystem response to phosphorus and nitrogen limitation in the Pearl River plume using the Regional Ocean Modeling System (ROMS), J. Geophys. Res., 119(12), 8858-8877, doi:10.1002/2014JC009951, 2014.

Garvine, R.W., and Monk, J.D.: Frontal structure of a river plume, J. Geophys. Res., 79(15), 2251-2259, 1974.

Geider, R., and Roche, J.: Redfield revisited: Variability of C:N:P in marine microalgae and its biochemical basis, Eur. J. Phycol., 37(1), 1-17, 2002.

Harrison, P.J., Yin, K., Lee, J.H.W., Gan, J., and Liu, H.: Physical-biological coupling in the Pearl River Estuary, Cont. Shelf Res., 28, 1405-1415, 2008.

Hillebrand, H., Steinert, G., Boersma, M., Malzahn, A., Meunier, C., Plum, C., and Ptacnik, R.: Goldman revisited: Faster-growing phytoplankton has lower N:P and lower stoichiometric flexibility, Limnol. Oceanogr., 58(6), 2076-2088, 2013.

Horner-Devine, A.R., Hetland, R.D., and Macdonald, D.G.: Mixing and transport in coastal river plumes, Ann. Rev. Fluid Mech., 47(47), 569-594, 2015.

Kies, K.: Distribution, biomass and production of planktonic and benthic algae in the Elbe Estuary, Limnologica, 27 (1), 55-64, 1997.

Knap, A., Michaels, A., Close, A., Ducklow, H., Dickson A.: Protocols for the Joint Global Ocean Flux Study (JGOFS) Core Measurements, JGOFS Report No 19, 170pp, 1996.

Li, Q. P., Franks, P.J.S., Ohman, M.D., and Landry, M.R.: Enhanced nitrate fluxes and biological processes at a frontal zone in the Southern California current system, J. Plankton Res., 34, 790–801, 2012.

Li Q. P., Dong, Y., and Wang, Y.: Phytoplankton dynamics driven by vertical nutrient fluxes during the

spring inter-monsoon period in the northeastern South China Sea, Biogeosci., 13, 1–12, 2016.

Litchman E, Klausmeier, C.A., Schofield, O.M., and Falkowski, P.G.: The role of functional traits and trade-offs in structuring phytoplankton communities: scaling from cellular to ecosystem level, Ecol. Lett., 10, 1170−1181, 2007.

Liu, K., Chao, S., Shaw, P., Gong, G., Chen, C., and Tang, T.: Monsoon-forced chlorophyll distribution and primary production in the South China Sea: observations and a numerical study, Deep-Sea Res. I, 49, 1387–1412, 2002.

St. Laurent, L.: Turbulent dissipation on the margins of the South China Sea, Geophys. Res. Lett., 35, L23615, doi:10.1029/2008GL035520, 2008.

Lohrenz, S.E., Redalje, D., Cai, W., Acker J., and Dagg, M.: A retrospective analysis of nutrients and phytoplankton productivity in the Mississippi River Plume, Cont. Shelf Res., 28(12), 1466-1475, 2008.

Mahaffey, C., Björkman, K.M., and Karl, D.M.: Phytoplankton response to deep seawater nutrient additions in the North Pacific Subtropical Gyre, Mar. Ecol. Prog. Ser, 460:13-34, 2012.

Marañón, E.: Cell size as a key determinant of phytoplankton metabolism and community structure, Ann. Rev. Mar. Sci., 7, 241–264, 2015

Marañón, E., Cermeño, P., Latasa, M., and Tad, R.D.: Temperature, resources, and phytoplankton size structure in the ocean, Limnol. Oceanogr., 57, 1266-1278, 2012.

Marañón, E., Cermeño, P., Latasa, M., and Tad, R.D.: Resource supply alone explains the variability of marine phytoplankton size structure, Limnol. Oceanogr., 60, 1848–1854, 2015.

McAndrew, P.M., Björkman, K.M., Church, M.J., et al.: Metabolic response of oligotrophic plankto communities to deep water nutrient enrichment, Mar. Ecol. Prog. Ser., 332, 63-75, 2007.

Moore, C.M., Mills, M.M., Arrigo, K.R., et al.: Processes and patterns of oceanic nutrient limitation, Nat. Geosci., 6(9), 701-710, 2013.

Morgan, C.A., Robertis, A.D., and Zabel, R.W.: Columbia River plume fronts. I. Hydrography, zooplankton distribution, and community composition, Mar. Ecol. Prog. Ser., 299, 19-31, 2005.

Ou, S., Zhang, H., and Wang, D.: Horizontal characteristics of buoyant plume off the Pear River Estuary during summer, J. Coast Res., 50, 652-657, 2007.

Raven, J.A.: The twelfth Transley Lecture. Small is beautiful: The picophytoplankton, Func. Ecol., 12, 503–513, 1998.

Su, J.: Overview of the South China Sea circulation and its influence on the coastal physical oceanography outside the Pearl River Estuary, Cont. Shelf Res., 24, 1745–1760, 2004.

Suttle CA, Cochlan, W.P., and Stockner, J.G.: Size-dependent ammonium and phosphate uptake, and N:P supply ratios in an Oligotrophic Lake, Can. J. Fish. & Aqua. Sci., 48(48), 1226-1234, 1991.

Vrede, T., Ballantyne, A.P., Millelindblom, C., Algesten, G., Gudasz, C., Lindahl, S., and Brunberg, A.K.: Effects of N:P loading ratios on phytoplankton community composition, primary production and N fixation in a eutrophic lake, Freshwater Biology, 54(2), 331-344, 2009.

Wong, L.A., Chen, J.C., Xue, H., Dong, L., Guan, W., and Su, J.: A model study of the circulation in the Pearl River Estuary and its adjacent coastal waters: 2 Sensitivity experiments, J. Geophys. Res., 108(C5), 249–260, 2003.

Wong, G. T., Tseng, C., Wen, L., Chung, S.: Nutrient dynamics and N-anomaly at the SEATS station, Deep-Sea Res. II, 54(54), 1528-1545, 2007.

Wu, J., Chung, S., Wen, L., Liu, K., Chen, Y.L., Chen, H., and Karl, D.M.: Dissolved inorganic phosphorus, dissolved iron, and Trichodesmium in the oligotrophic South China Sea, Global Biogeochem. Cycle, 17(1), 1008–1016, 2003.

Yin, K., Qian, P., Wu, M., Chen, J., Huang, L., Song, X., and Jian W.: Shift from P to N limitation of phytoplankton biomass across the Pearl River estuarine plume during summer, Mar. Ecol. Prog. Ser., 221: 17-28, 2001.

Zhang, J., Yu, Z., Wang, J., Ren, J., Chen, H, Xiong, H., Dong, L., and Xu, W.: The subtropical Zhujiang (PearlRiver) Estuary: nutrient, trace species and their relationship to photosynthesis, Estuar. Coast. Shelf Sci., 49(3), 385–400, 1999.

Table 1. Hydrographic and biogeochemical properties of the surface and bottom waters for incubations over the NSCS shelf during May and June 2016. Nutrient addition experiments and water mixing experiments were conducted immediately after we reached these stations.

Station	Date	Depth [m]*	T [°C]	S [‰]	Chl-*a* [μg L⁻¹]	micro [%]	nano [%]	pico [%]	Si [μM]	N+N [μM]	SRP [μM]	N/P
S1	5/18	1	24.5	20.4	7.01	73.8	14.3	11.9	34.1	33.3	0.22	151
		10	23.6	31.7	7.93	37.4	5.6	56.9	16.4	20.1	0.32	63
S2	6/19	1	29.1	6.6	6.82	19.9	65.8	14.2	192.5	80.4	0.83	97
		8	25.6	34.0	0.31	12.1	65.3	22.5	43.9	16.7	0.65	28
S3	5/15	1	27.9	30.9	0.91	35.3	39.2	25.5	3.2	16.6	0.13	127
		50	20.9	34.5	0.34	17.9	43.2	38.9	4.3	7.7	0.22	35
S4	6/18	1	30.0	30.7	1.24	5.5	43.8	50.7	1.2	6.6	0.21	32
		39	21.7	34.6	0.91	4.9	32.6	62.5	10.8	6.1	0.23	26
S5	5/19	1	26.6	34.4	0.26	1.3	8.8	89.9	1.4	1.0	0.09	12
		36	23.8	34.3	0.15	15.0	27.9	57.1	2.0	1.3	0.11	11
S6	6/19	1	30.7	34.5	0.73	0.3	23.8	75.8	2.2	0.5	0.14	3
		47	21.7	34.7	0.45	9.2	21.0	69.8	9.3	3.6	0.17	21
S7	6/21	1	30.8	32.1	0.59	0.7	45.1	54.2	1.3	3.3	0.07	46
		109	19.2	34.7	0.07	1.4	11.0	87.6	13.3	9.2	0.61	15
S8	6/27	1	31.3	30.9	0.33	10.0	44.7	45.3	2.65	3.0	0.18	17
		39	21.7	34.6	0.91	4.85	32.9	64.7	6.69	4.9	0.27	18

*The depth of surface water is always at ~1 m with the depth of bottom water 5-10 m above the topography.
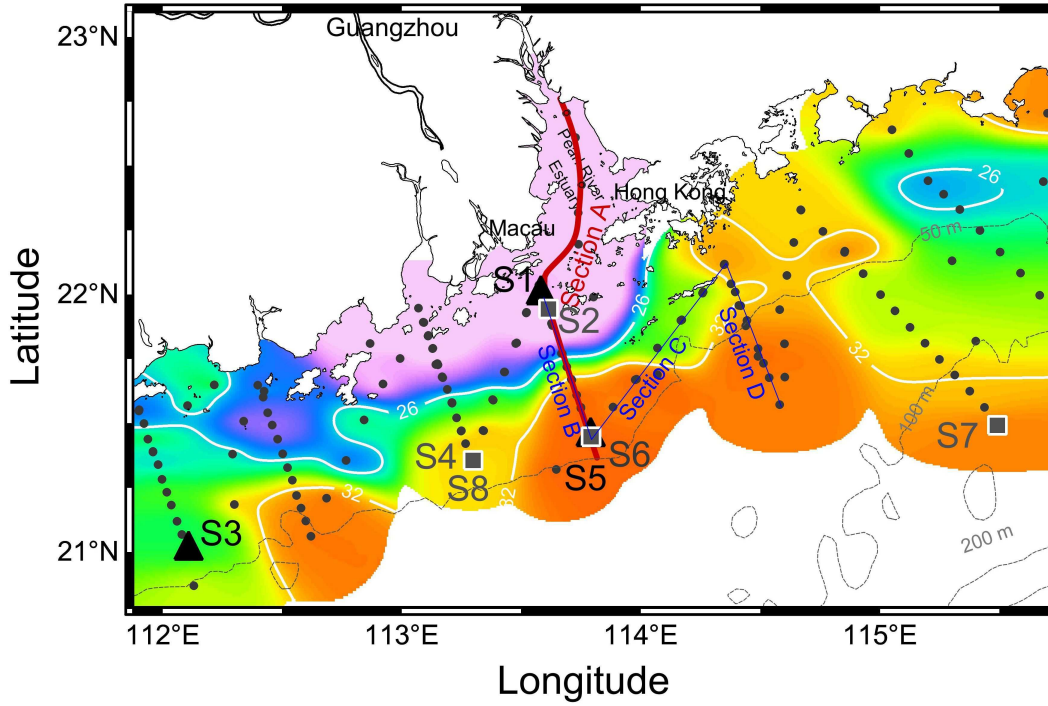
4   **Figure 1.** Sampling map in the NSCS shelf during May-June 2016. Color is the surface salinity of three

5   cruises with the frontal zone by white lines of 26 and 32 (nearshore and offshore boundaries of the

6   plume); Section A across the front from the PRE to the shelf; section B across the front with sections C

7   and D on the seaside; triangles are incubation sites S1, S3, S5 during May 2016 and squares are

8   incubation sites S2, S4, S6, S7, and S8 during June 2016; locations of S6 and S8 are overlaid with S5

9   and S4, respectively; dots are the stations with dash lines the isobaths.
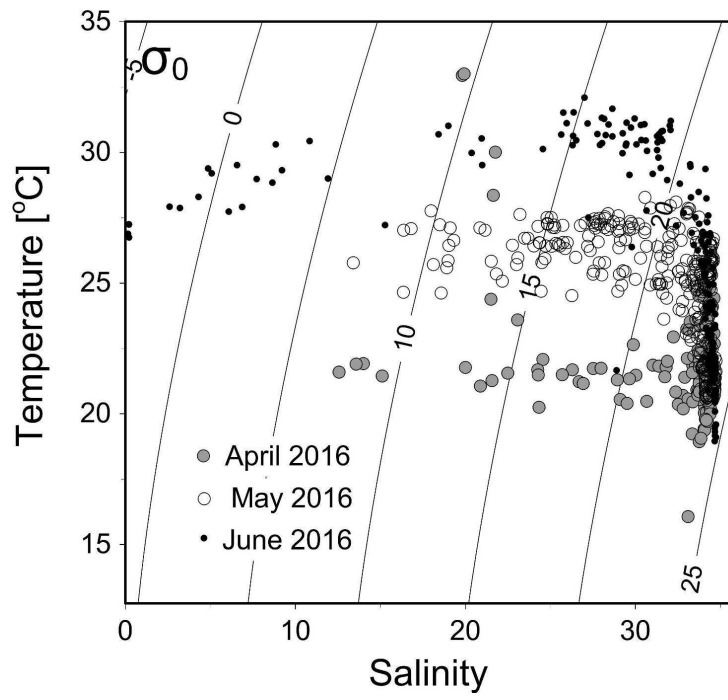
Figure 2. A Temperature vs. Salinity diagram during April-June 2016. Filled circles, open circles, and dots are data of April, May, and June cruises, respectively.
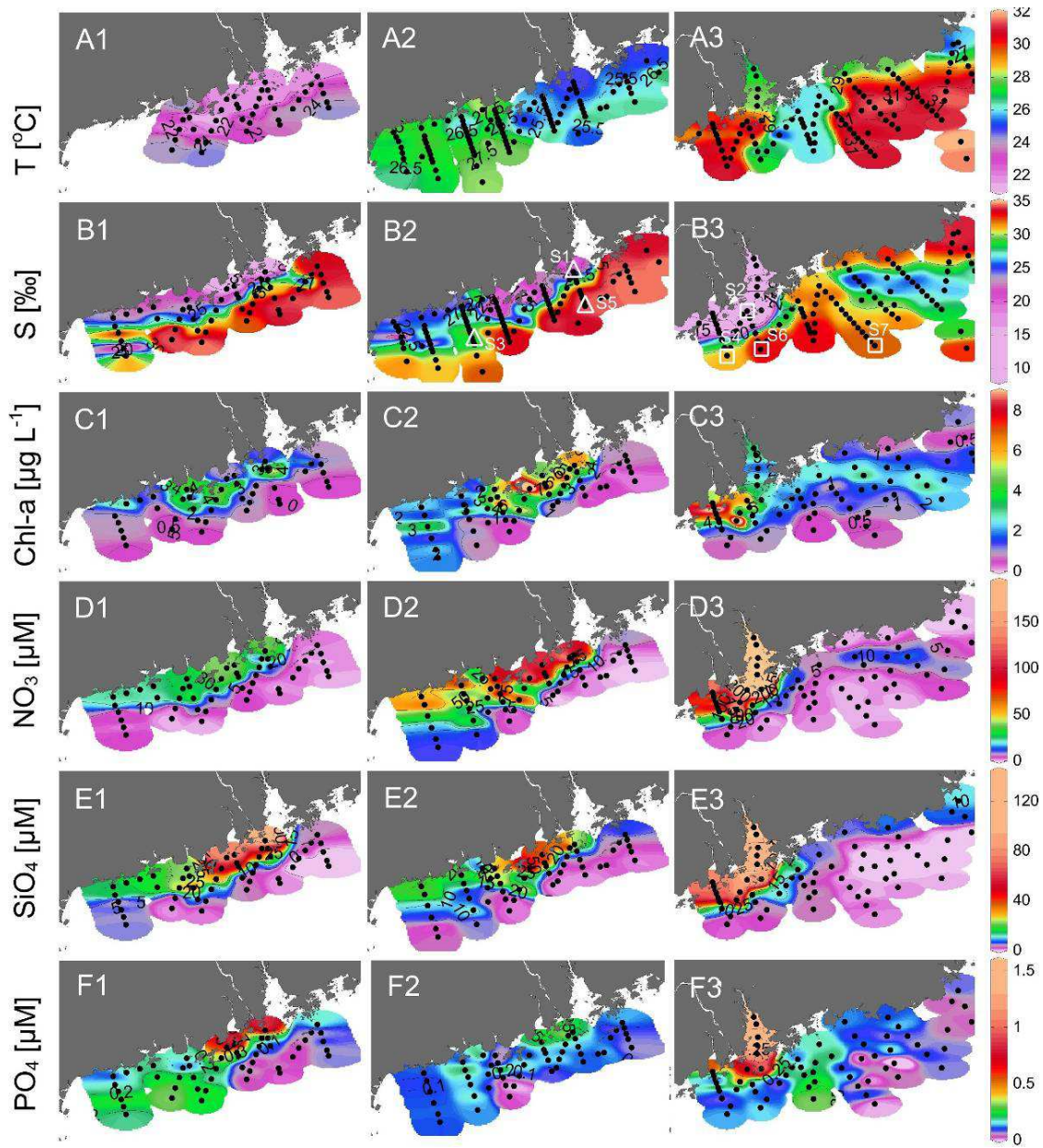
Figure 3. Surface distributions of **(A1-A3)** temperature, **(B1-B3)** salinity, **(C1-C3)** chlorophyll-*a*, **(D1-D3)** nitrate, **(E1-E3)** silicate, and **(F1-F3)** phosphate in the NSCS during April, May, and June 2016. Small dots are the data points; open triangles and squares in B2-B3 show the positions of S1-S7.
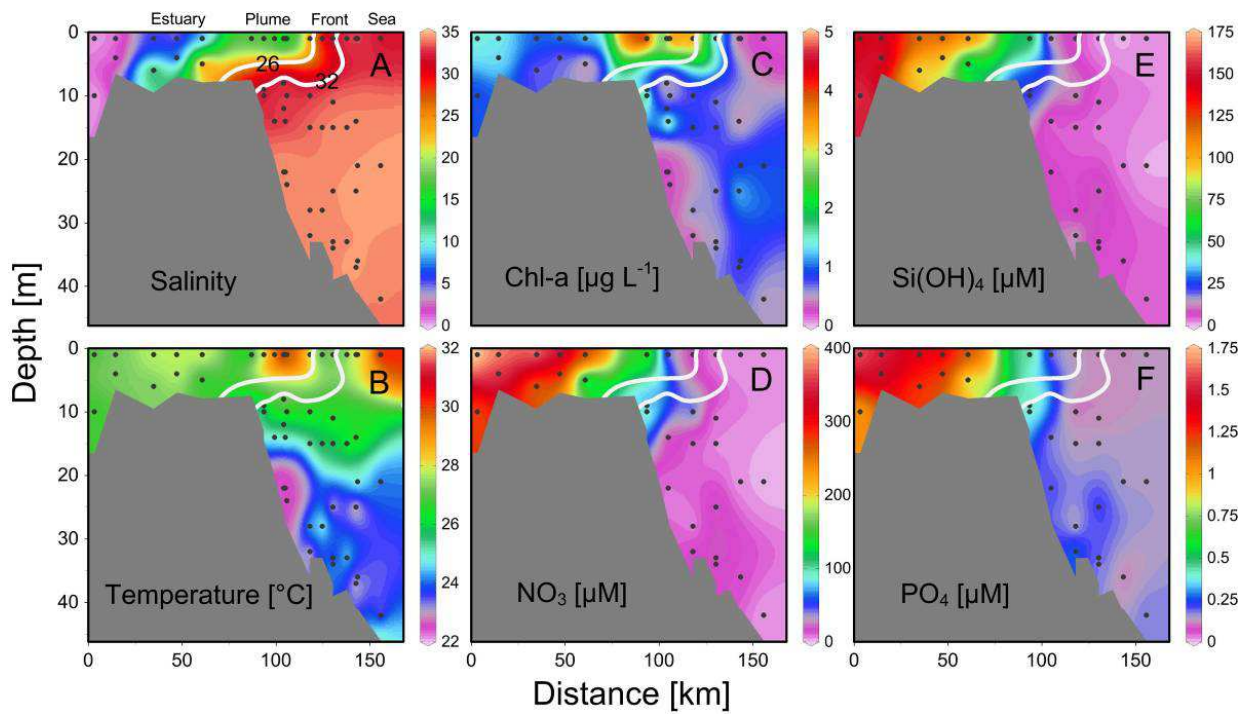
Figure 4. Vertical distribution of **(A)** salinity, **(B)** temperature, **(C)** chlorophyll-*a*, and **(D)** nitrate, **(E)** silicate, and **(F)** phosphate across the front from the estuary to the sea. Location of the section during the three cruises is in Fig.1. Two white lines overlaid are salinity of 26 and 32 for nearshore and offshore boundaries of the plume (see text for detail).
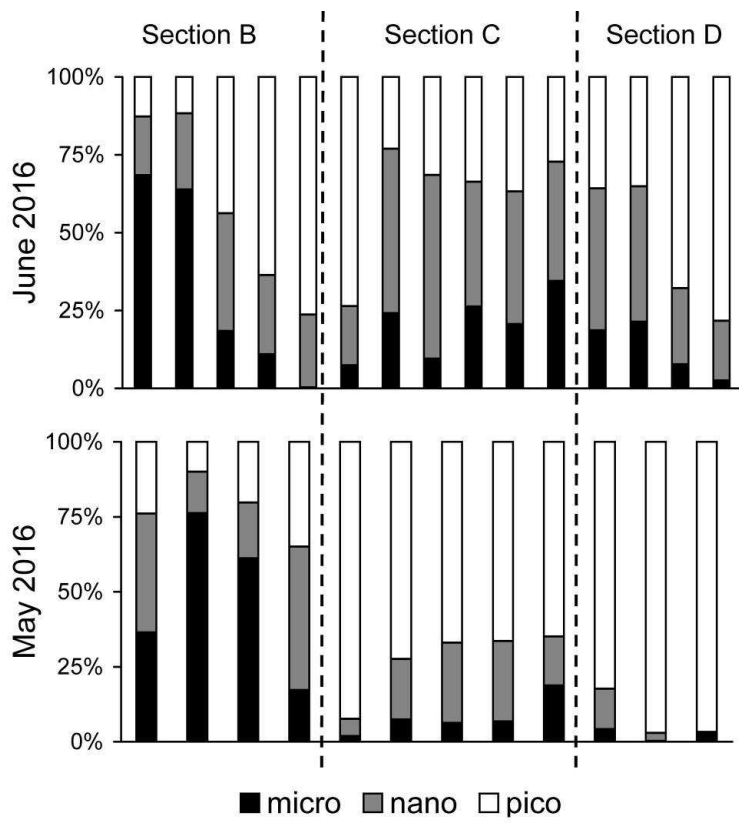
3 **Figure 5.** Comparisons of size-fractionation chlorophyll-*a* for sections B, C, and D between May and

4 June 2016.
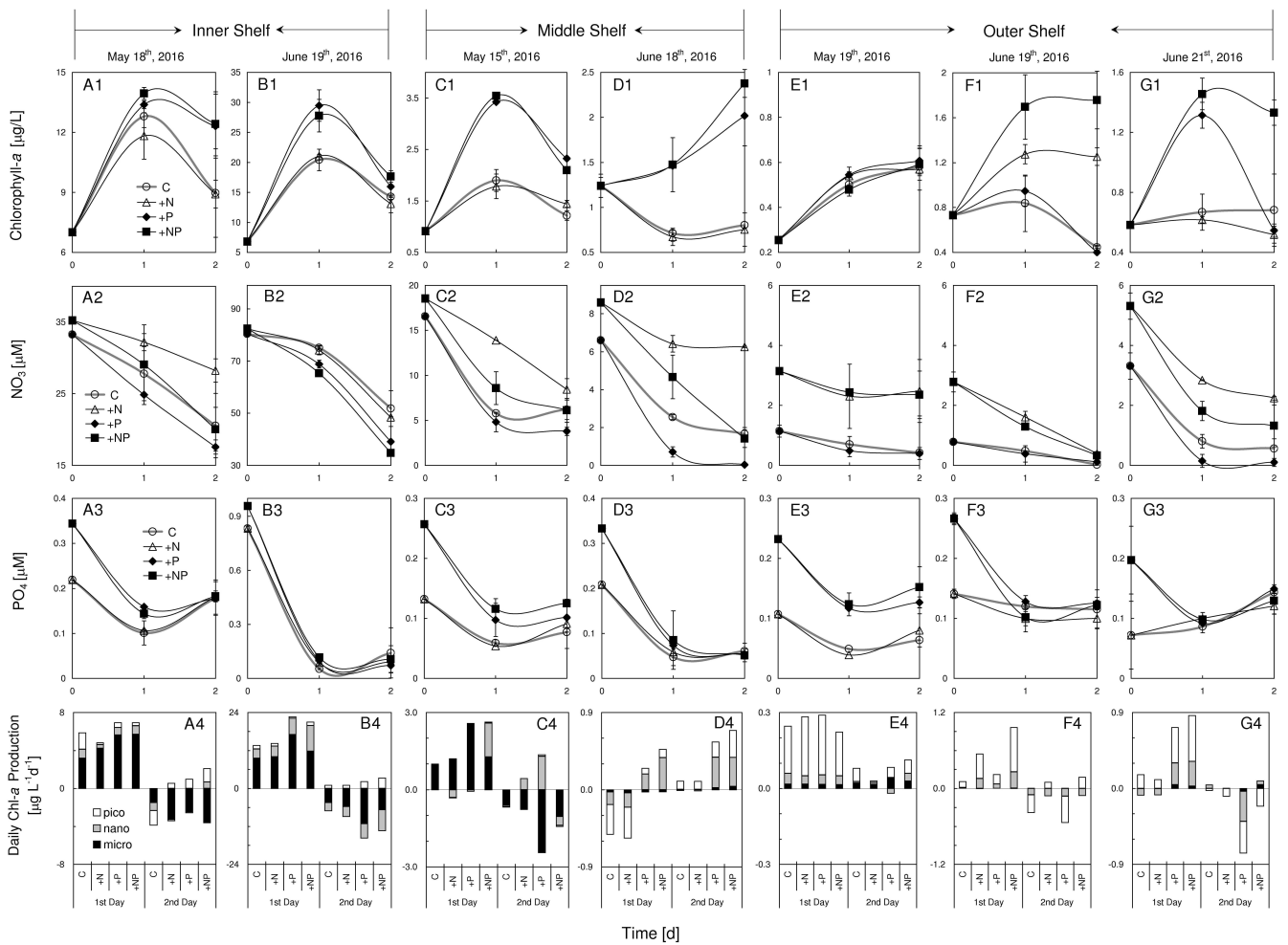
3 **Figure 6.** Responses of total chlorophyll-*a*, nitrate, phosphate, and size-fractionated daily chlorophyll-*a*

4 production rate of the surface water to various nutrient enrichments at **(A1-A4)** S1, **(B1-B4)** S2, **(C1-C4)**

5 S3, **(D1-D4)** S4, **(E1-E4)** S5, **(F1-F4)** S6, and **(G1-G4)** S7 during May and June 2016. Station locations

6 are in Figure 1 with the initial conditions in Table 1; Treatments include control (C), nitrogen alone

7 (+N), phosphorus alone (+P), and nitrogen plus phosphorus (+NP), respectively; Chlorophyll-*a* size

8 fractionations of the initial waters for these stations are shown in Table 1.
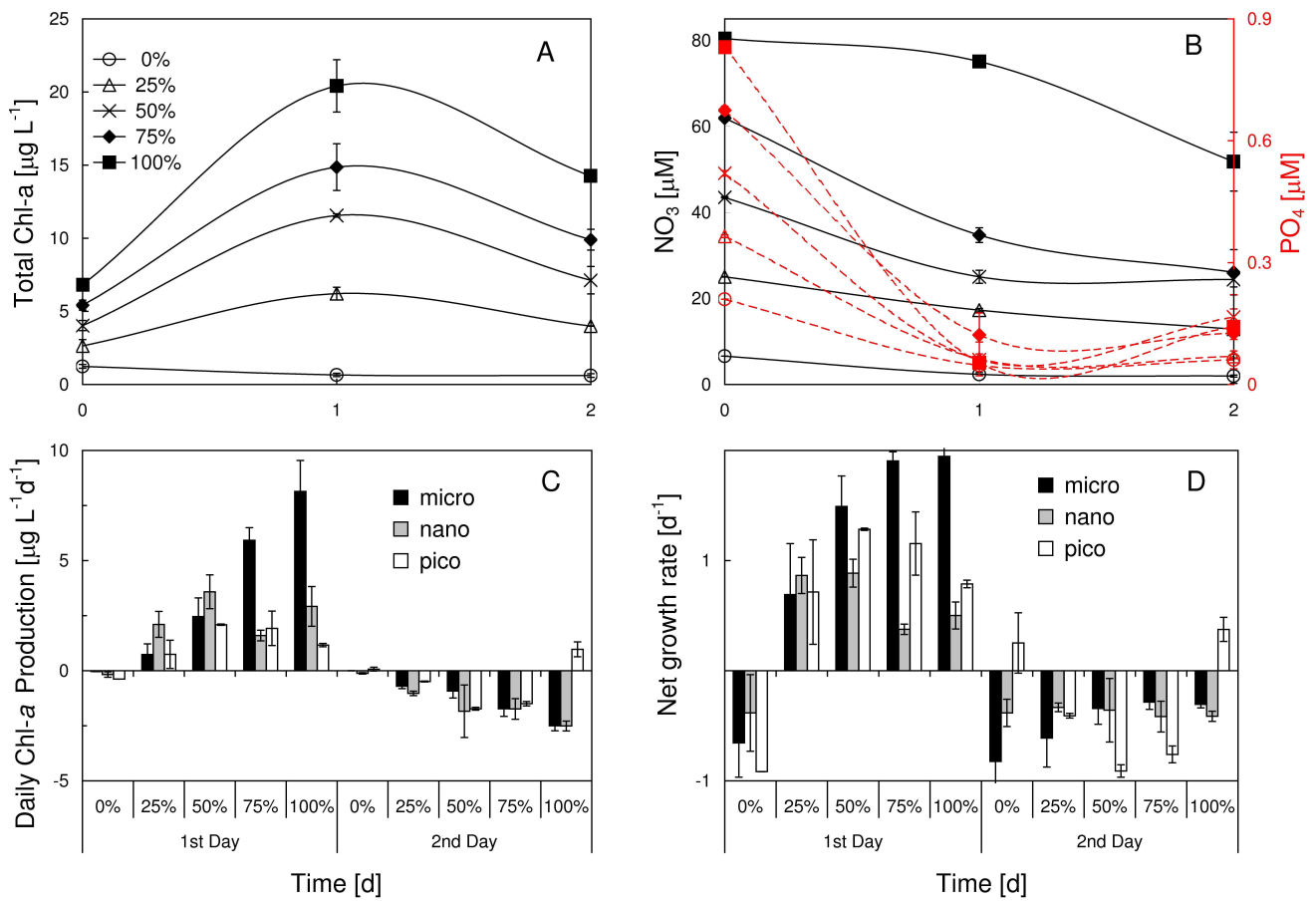
Figure 7. Responses of **(A)** total chlorophyll-*a*, **(B)** nitrate and phosphate, **(C)** size-fractionated rate of daily chlorophyll-*a* production, and **(D)** size-fractionated net growth rate of the surface water at S4 to a varying percentage of plume water from S2. The experiment was started on June 19th, 2016.
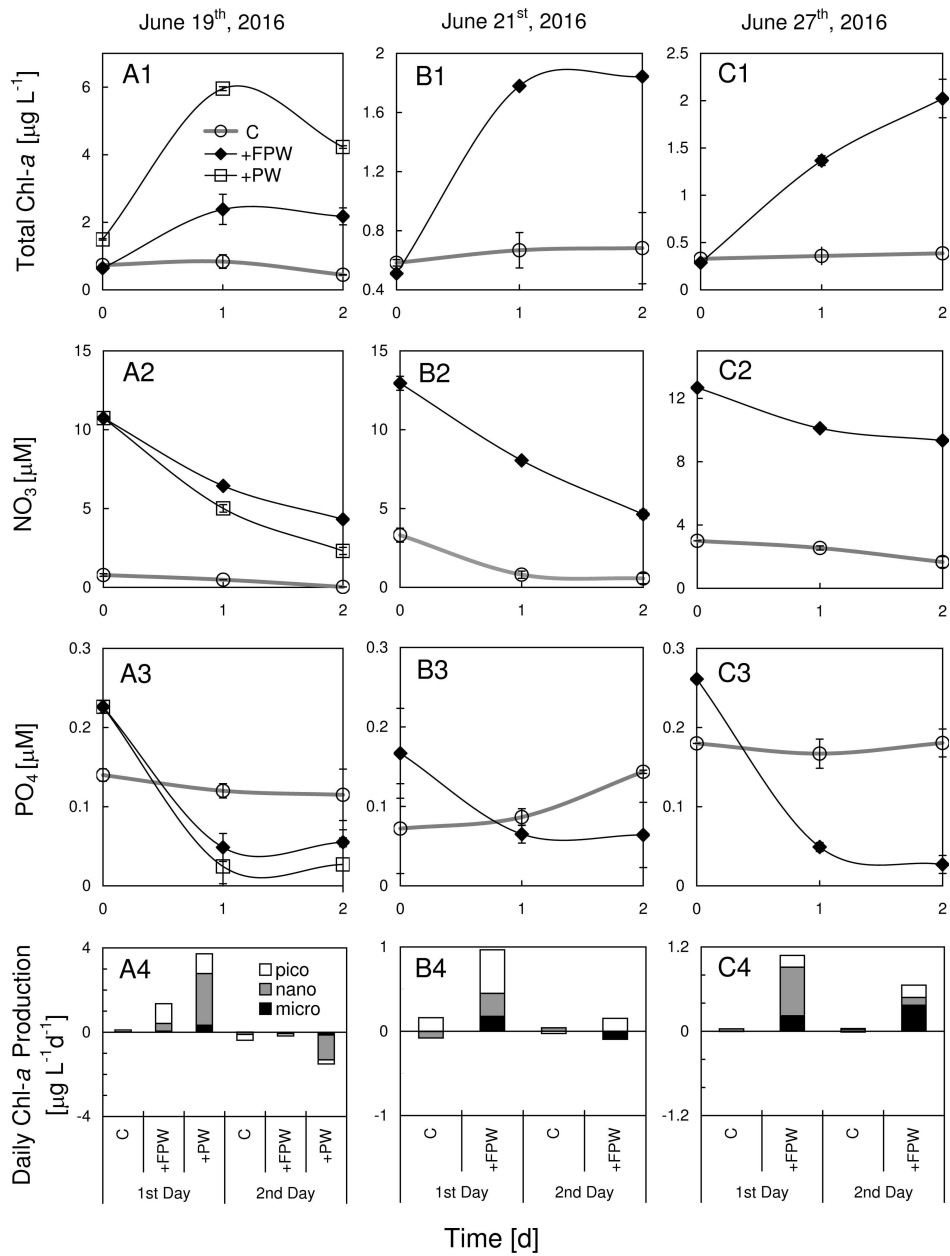
Figure 8. Responses of total chlorophyll-*a*, nitrate, phosphate, and size-fractionated rate of daily chlorophyll-*a* production of the surface water to the addition of plume water at **(A1-A4)** S6, **(B1-B4)** S7, and **(C1-C4)** S8. PW is the plume water with FPW the filtered plume water.
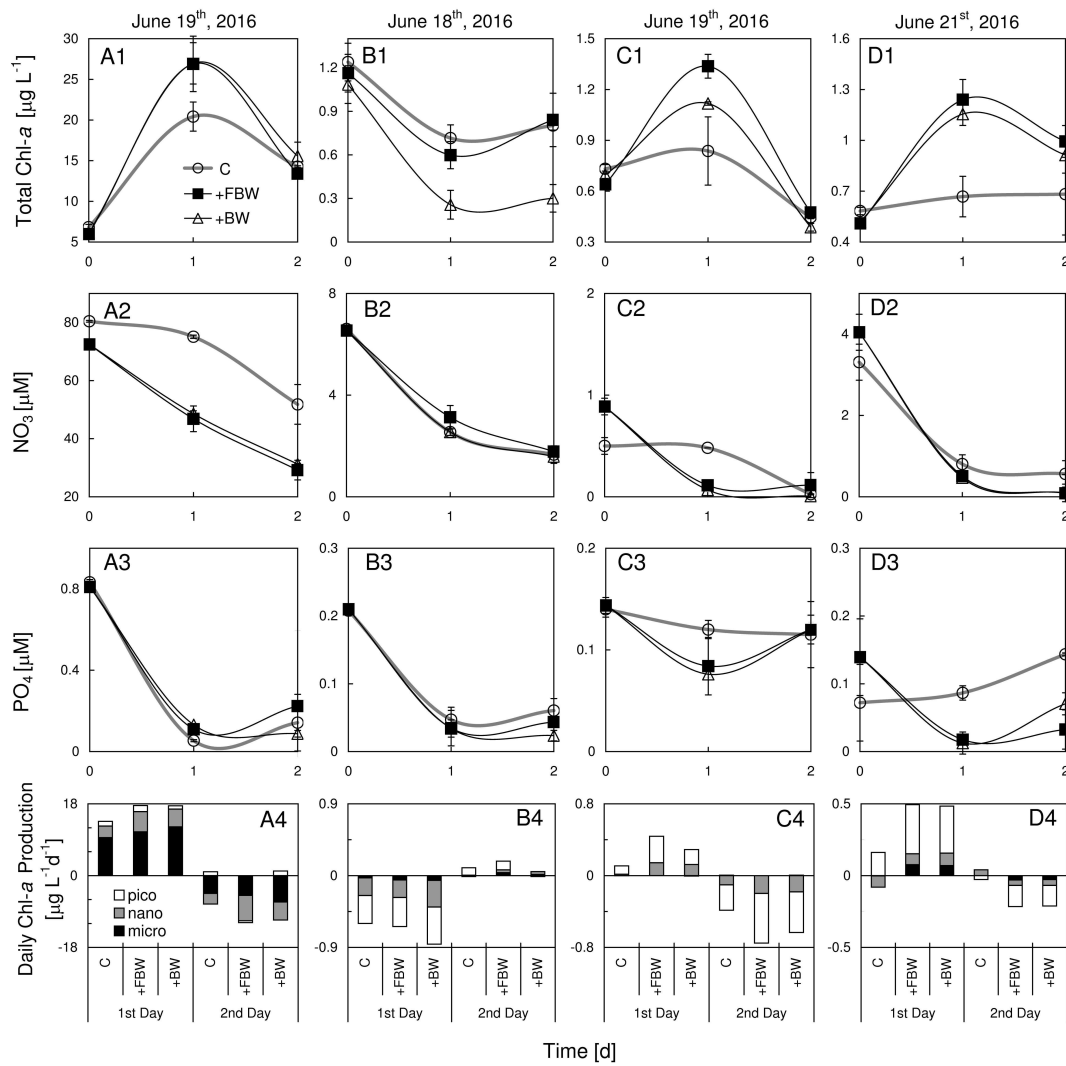
Figure 9. Responses of total chlorophyll-*a*, nitrate, phosphate, and size-fractionated rate of daily chlorophyll-*a* production of the surface water to the addition of local bottom waters at stations **(A1-A4)** S2, **(B1-B4)** S4, **(C1-C4)** S6, and **(D1-D4)** S7 during June 2016. BW is the bottom water with FBW the filtered bottom water.